ADVANCES IN ATMOSPHERIC SCIENCES, VOL. 22, NO. 2, 2005, 260–270

AREM Simulations of Cloud Features over Eastern China in February 2001

LI Yunying*[1,2] (李昀英), YU Rucong*[1,3] (宇如聪), XU Youping[1] (徐幼平), and ZHOU Tianjun[1] (周天军)

[1] *State Key Laboratory of Numerical Modeling for Atmospheric Sciences and Geophysical Fluid Dynamics, Institute of Atmospheric Physics, Chinese Academy of Sciences, Beijing* 100029

[2] *Institute of Meteorology, PLA University of Science and Technology, Nanjing* 211101

[3] *China Meteorological Administration, Beijing* 100081

(Received 22 June 2004; revised 1 December 2004)

ABSTRACT

Based on the simulations of cloud features in February 2001 by the regional numerical weather prediction model—Advanced Regional Eta-coordinate Model (AREM), the dynamic and thermodynamic conditions for middle cloud formation over eastern China are studied. Diagnostic analysis partly confirms the previous suggestion that the middle stratiform clouds downstream of the Tibetan Plateau are maintained by the frictional and blocking effects of the plateau. In addition, it is found that the temperature inversion at plateau height over eastern China generated by the warm air advected from the plateau provides a favorable thermodynamic condition for middle clouds. Both diurnal variations of the mid-level divergence and the inversion over eastern China, which are determined by the atmospheric boundary activity over the Tibetan Plateau, dominate the cloud diurnal cycle. The middle cloud amount decreases and the cloud top falls in the daytime, but reverses at night. The comparison of cloud features between the simulations and the observations also proves that the AREM can well capture the distinctive continental stratiform cloud features downstream of the Tibetan Plateau.

Key words: AREM, eastern China, middle cloud, divergence, inversion

1. Introduction

Eastern China (EC) is one of the cloudiest regions in the world (Klein and Hartmann, 1993), the dominating optically thick middle stratiform clouds in cold seasons affect the regional weather and climate seriously. However, only little attention has been paid to the continental mid-level clouds. Using the ISCCP (International Satellite Cloud Climatology Project) cloud data and ECMWF (European Centre for Medium-Range Weather Forecasts) reanalysis data, Yu et al. (2001) showed the special cloud characteristics over EC by the globally largest nimbostratus cloud amount, and related it to the mid-troposphere divergence generated by the friction of the Tibetan Plateau on the passing through westerly. To further explain some features and the formation mechanism of the middle stratiform clouds over EC, a regional numerical prediction model AREM (Advanced Regional Eta-coordinate Model, Yu et al., 2004) is used, and some new findings are shown in this paper.

The REM (Regional Eta-coordinate Model, Yu et al., 1994), a previous version of the AREM, is one of the widely used numerical weather forecasting models in China. Its usage includes heavy rainfall prediction, drought evaluation and environmental pollution simulation, etc. (Zhong and Qing, 2001; Ju et al., 2003; Zhang et al., 2003). Recently REM was upgraded and renamed AREM. The resolution, lateral boundary condition, initial fields and standardization and modularization of the model were greatly improved. Many physical processes were also replaced by advanced ones. An explicit prognostic cloud scheme (Xu et al., 1998), which predicted the generation rates of water vapor, cloud water and rain, was one of the distinct improvements in the AREM. Based on the new cloud scheme, we introduce a diagnostic cloudiness scheme (Xu and Randall, 1996) into AREM, providing cloud amount for the radiation parameterization.

*E-mail: yrc@lasg.iap.ac.cn

A complete cloud-radiation-precipitation process is established in the AREM and further studies on cloud processes can be carried out. In this paper, the performance of the AREM on mid-cloud features over China is evaluated.

In general, total cloud amount and high, middle, and low cloud fractions are calculated by an overlapping method in the model. However, clouds are defined by the base height in surface observations, and by the top height in satellite observations. Both definitions are different from that used in models, which causes the difficulty that the "model cloud" cannot be easily compared with either the surface data or the satellite data such as ISCCP (Rossow and Schiffer, 1991; Doutriaux-Boucher and Seze, 1998; Rossow and Schiffer, 1999). The ISCCP D1 dataset can provide global cloud distribution every 3 hours for each day from 1 July 1983 to 30 September 2001. If clouds defined by the models are converted to clouds defined by ISCCP, the "model clouds" can be compared with the ISCCP data quantitatively. One conversion technique called the "ISCCP cloud simulator" has been developed. Using this conversion method, some comparison work on GCMs has been done (Webb et al., 2001; Williams et al., 2003; Lin and Zhang, 2004; Weare, 2004). In this study, the "ISCCP cloud simulator" is added to the AREM to examine the model cloud simulation quantitatively.

An integration for February 2001 by the AREM model is selected as a test case for our study. February is chosen because it is the month with the largest middle cloudiness in the year (Li et al., 2004), and 2001 is selected since it is the latest year available in the ISCCP dataset. The rest of the paper is organized as follows. Section 2 introduces the AREM model and cloud diagnostic and output methods. Section 3 examines the model performance in simulating the cloud features. The dynamic and thermodynamic conditions for middle clouds over EC are analyzed in section 4, and a brief summary is presented in the last section.

2. Description of AREM and cloud diagnostic and output methods

2.1 *Description of AREM and the integration method*

AREM is a regional mesoscale weather forecasting model. Its key features are highlighted here. The Arakawa E-grid scheme is selected as the model horizontal grid structure. The Eta-coordinate is adopted as the vertical coordinate, and the diagnostic geopotential and vertical velocity are defined at the interface of the vertical levels against other prognostic variables. The departures of temperature, geopotential height and surface pressure from their "standards" are used in the prediction equations to increase the calculation precision. A "half-space-increment" finite-difference is used to improve the accuracy of the advection difference in the E-grid, a two-step, shape-preserving advection scheme (Yu, 1994) is designed to keep a reasonable moisture advection, and a split explicit scheme is used in the time integration to make it possible for each part in a set of equations to have its own suitable finite-difference scheme. The model domain, horizontal and vertical resolution and top height can all be adjusted. The physical processes can also be selected from several schemes, and the lateral boundary condition can be fixed or vary with time.

The model specifics for this study are set as follows: the domain covers 15°–55°N, 85°–135°E, with about 37-km horizontal resolution and 36 uneven levels in the vertical from the surface to 10 hPa. The physical processes include the explicit prognostic warm cloud scheme (Xu et al., 1998), modified Betts (1986) convective adjustment scheme, a non-local diffusion boundary layer parameterization scheme (Holtslag and Boville, 1993), and a radiation scheme (Edwards and Slingo, 1996; Sun and Rikus, 1999). A CLM (Column Land Model, Dai and Zeng, 1998) is also coupled with AREM.

The NCEP $1^\circ \times 1^\circ$ reanalysis data are taken as the initial fields and lateral boundary condition. The 12-hourly data are used to update the model lateral boundary condition. A one-way nesting condition is used and the buffer zone is 5° near the lateral boundaries, within which the model prognostic variables are nudged to the reanalysis data. The weekly SST (Reynolds et al., 2002) interpolated to daily mean data are used as external forcing, with no diurnal cycle. Under the time-varying lateral boundary condition and observed SST forcing, the model is integrated from 0000 UTC 31 January 2001 to 2400 UTC 28 February 2001, outputting every 3 hours. Note that the first day is considered as a spinup stage and excluded from our analysis. The time in this paper is defined by Universal Time (UTC).

2.2 *Diagnostic cloudiness scheme*

In the diagnostic cloudiness scheme (Xu and Randall, 1996), the cloud amount is determined by both relative humidity and cloud water-ice mixing ratio,

$$C_k = \begin{cases} R_{\rm H}^p\{1-\exp\{-\alpha q/[(1-R_{\rm H})q_*]^\gamma\}\} & \text{if } R_{\rm H} < 1\,, \\ 1 & \text{if } R_{\rm H} \geqslant 1\,, \end{cases} \tag{1}$$

where C_k is cloud fraction at model level k, $R_{\rm H}$ is relative humidity, q is total mixing ratio of cloud water

and cloud ice, q_* is saturated water vapor mixing ratio, p, α, γ are constants and taken to be 0.25, 100 and 0.49, respectively.

This diagnostic scheme is significantly different from others that are mainly dependent on $R_{\rm H}$. Here $R_{\rm H}$ is only used to adjust the slope of the relationship between the cloudiness and cloud water-ice mixing ratio. Siebesma et al. (2003) showed that this representation was satisfactory for marine stratiform clouds. However, according to our pre-simulation, the model cloud amount over China is systematically smaller than observation. Because of the resolution difference between AREM and the model used by Xu and Randall (1996), the constant α is adjusted to 400 in this study.

2.3 *Cloud overlapping assumption*

There are three methods to calculate the total cloud amount from cloud fraction available at each model level, and the maximum-random assumption (Morcrette and Fouquart, 1986) is taken in our study. It uses a random assumption for clouds that do not occur at adjacent vertical levels, but a maximum assumption if clouds occur at adjacent levels with cloud fraction monotonically increasing or decreasing with height.

In the AREM, high clouds are defined as clouds occurring above the 440-hPa level, low clouds are defined as clouds occurring below the 680-hPa level, and middle clouds are in between. Note that the total cloud amount is obtained using the maximum-random assumption from all model levels, and the high, mid and low-level cloud fractions are only obtained from model levels within their individual pressures. It is obvious that the definition of the "model cloud" is different from that of the ISCCP data in which cloud heights are defined by cloud top pressures. For example, if clouds develop from low to high levels continuously, it is considered that low, mid and high-level clouds co-exist in the model, but the cloud would be considered as high-level cloud in the ISCCP data. So only if the "model cloud" is converted to "ISCCP cloud" can these two kinds of cloudiness be compared with each other quantitatively.

2.4 *ISCCP simulator*

For the ISCCP data, a grid area is about 280 km×280 km and is further divided into many pixels. The cloud amount is the ratio of the sum of the cloudy pixel area to the grid area. Clouds are classified into 42 types based on cloud top pressure (PC, 7 categories) and cloud optical depth (TAU, 6 categories) as shown in Fig. 1. The fraction of each cloud type is available in the ISCCP D1 dataset.

In order to compare the model cloudiness with the ISCCP data, the "ISCCP cloud simulator" is added into the AREM. The "ISCCP cloud simulator" mimics the satellite observation of clouds by taking the cloud and atmospheric information from the model and generating cloud information that would have been observed by a satellite from space. It is available from http://isccp.giss.nasa.gov. It is now running in some models such as the Hadley Centre, NCAR, BMRC and CSU models. Clouds at each model layer are first downscaled to cloudy or cloud-free sub-columns. The columns are then vertically aligned with the overlapping assumption consistent with the radiation routine in the model. The cloud top is specified as the top pressure of the sub-column cloudy layer, and the optical depth of each sub-column is the sum of all cloudy layer optical depth. Finally, the frequencies in different bins of cloud optical depths and cloud top pressures are used to compare with satellite measurements as shown in Fig. 1. Because only visible optical depths are available in the ISCCP data, the converted cloud amount of various types can only be compared in the daytime.

3. Simulation of cloud features over eastern China in February 2001

3.1 *Cloud distributions*

Stratiform cloud is the dominant cloud type over China in cold seasons. The middle stratiform clouds mainly occur over eastern China (25°–35°N, 102.5°–122.5°E), and low stratiform clouds mainly occur over southeastern China (20°–25°N, 110°–125°E) (Li et al., 2003). The model domain and regions of interest are

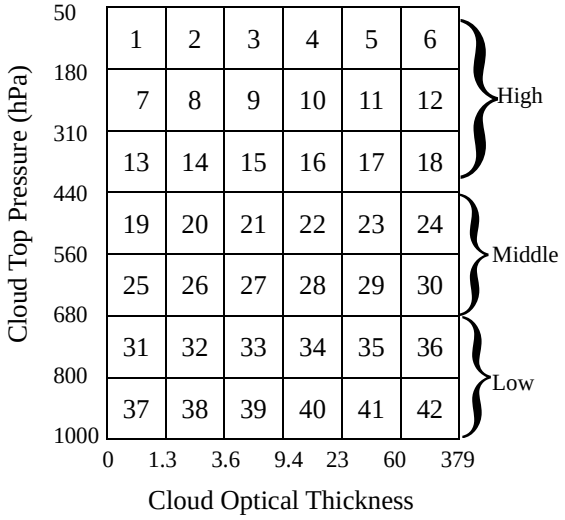

Fig. 1. ISCCP D1 Cloud Classification.

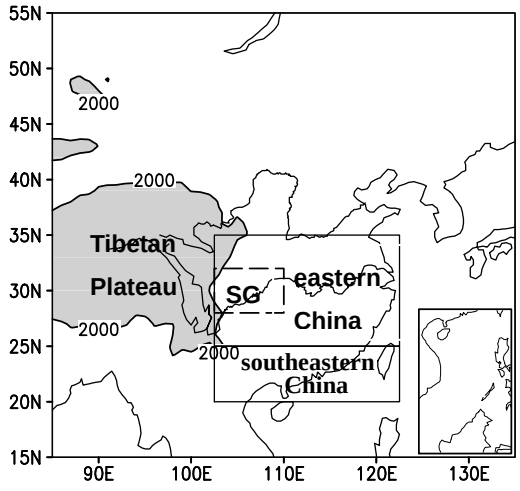

Fig. 2. The model domain (15°–55°N, 85°–135°E) and regions of interest such as eastern China (25°–35°N, 102.5°–122.5°E), southeastern China (20°–25°N, 102.5°–122.5°E), and the SG region (28°–32°N, 102.5°–110°E). The shading indicates where the topography is higher than 2000 m.

shown in Fig. 2 to facilitate discussions. Figures 3a and 3b show monthly mean observed and simulated middle cloud amount over China in February 2001, respectively. It is shown that the AREM model can reproduce the basic pattern of mid-level cloud amount over China. Figure 3b clearly reveals the larger cloud amount over the region 28°–32°N,102.5°–110°E, (hence called the SG region) and the smaller cloud amount over southeastern China. It also reveals an interesting phenomenon that all large middle cloud amount centers appear on the windward side of the Tibetan Plateau, which agrees well with the ISCCP observations. However, the simulated cloud center is too close to the Plateau, resulting in a significant underestimation over the lower reaches of the Yangtze River. In spite of these discrepancies, their patterns are similar.

To further compare the cloud features of the AREM with the ISCCP data quantitatively, the "model cloud" is converted to "ISCCP cloud". Figures 4a and 4b show the results of such a comparison over SG region at 0300 and 0600 UTC in February 2001, respectively. The differences between the model and the observed data are evident. The model cloud top heights are lower than the observations, cloud amounts at both times are underestimated, and cloud optical depths are overestimated. Because ISCCP cloud top is defined as the interval between two pressure levels, e.g., 560–440 hPa, we cannot tell exactly how much the simulated pressure is lower than the observation. It is possible the disagreement is attributable to deficiencies in the model simulation. However, over eastern China, where the temperature in the middle and lower atmosphere is significantly lower than that elsewhere at the same latitude, the ISCCP cloud height, which is calculated by the cloud temperature using the atmospheric temperature profile, may be overestimated. In spite of these disagreements, the cloud basic structures are captured by the AREM model.

3.2 *Diurnal cycle of cloudiness*

Cloudiness over EC displays a distinct diurnal cycle. Figures 5a and 5b show the monthly mean diurnal cycle of the cloudiness over SG region in February 2001

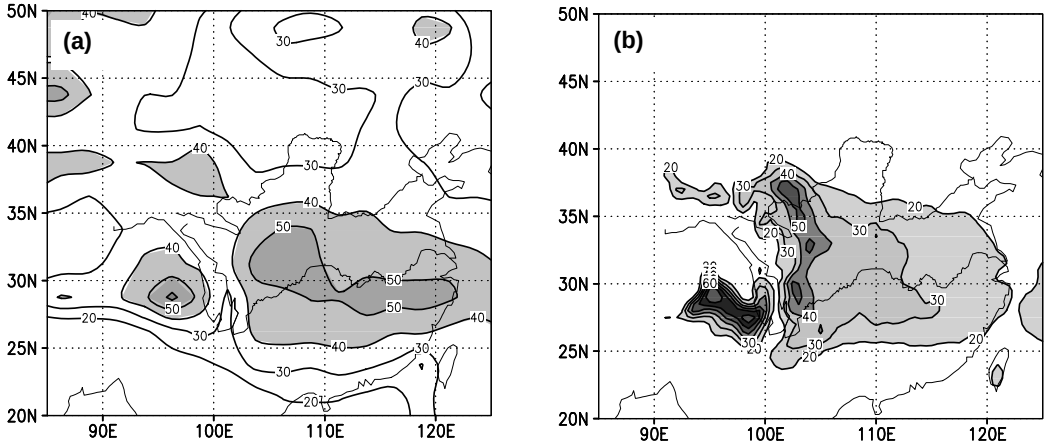

Fig. 3. Spatial distribution of monthly mean middle cloud amount (in %) in February 2001 derived from (a) the ISCCP D1 data and (b) the AREM model. Values larger than 40% in (a) and 20% in (b) are shaded.

derived from the ISCCP data and the AREM model, respectively. The two figures show similar diurnal changes of vertical cloud fraction, as cloud amount decreasing and top falling in the daytime, increasing and top rising at night. Although the model cloud height is lower than observation, the diurnal cycle is simulated quite well.

In conclusion, the essential features of middle cloud and its diurnal cycle are reproduced well by the AREM model, which provides a good basis for later analysis.

4. Dynamic and thermodynamic conditions for middle stratiform clouds

The Tibetan Plateau plays an important role in the weather and climate in China, and even in the world. The formation and variation of middle clouds over EC, which is located downstream of the Tibetan Plateau, may also be related to the dynamic and thermodynamic effects of the huge topography.

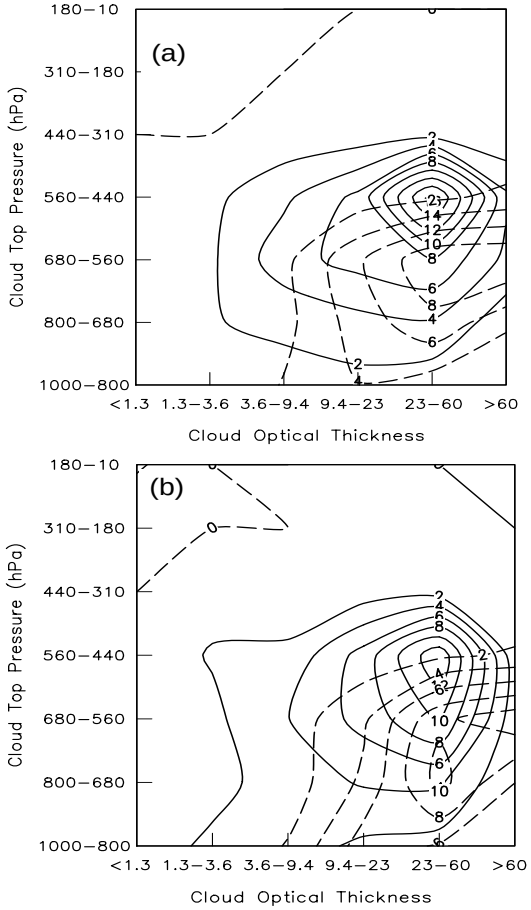

Fig. 4. Frequency distribution (in %) of monthly mean cloud optical thickness versus cloud top pressure averaged over the SG region in February 2001 at (a) 0300 UTC and (b) 0600 UTC derived from the ISCCP D1 data (solid line) and the AREM model (dashed line).

4.1 *Dynamical circulation in the low and middle troposphere*

The round flows from the north and south of the plateau converge over EC in the cold seasons. The location of the convergence is also determined by the strength of the winter monsoon. When the winter monsoon is strong, the northerly flow may dominate the whole of China; when it is weak, the southwesterly may invade to the Yangtze River in the middle atmosphere. In February 2001, the monthly mean convergence belt is located in the regions along the Yangtze River at 700 hPa. A weak cyclonic circulation controls SG region and the upward motion dominates the whole of eastern China in the middle troposphere (figure not shown). Moreover, because of the existence of water vapor sources such as the South China Sea, the East China Sea and favorable wind direction in winter in the low troposphere, the precipitable water in the lower atmosphere over EC is very large, especially in SG region where the highest relative humidity in the cold seasons exists in China (figures not shown). With abundant water vapor and large-scale upward motion, stratiform clouds can easily form over EC. In addition, there exists local circulation over EC. Figure 6 shows the simulated monthly mean vertical circulation along 30°N in February 2001. In the cold seasons, the easterlies dominate the regions along 30°N in the lower atmosphere. When the easterlies are held up by the north-south oriented mountains such as the Dalou Shan or Wu Shan mountains located in the eastern part of the Sichuan Basin, the air climbs up, flows over the mountains, and subsides on the lee side of the mountains. Moreover, when low-level easterlies intrude into the western part of the Sichuan Basin, the air climbs up along the slope of the Tibetan Plateau. The upward flows gradually turn to the east and become westerly flows in the middle troposphere. Thus a secondary circulation with ascending motion in the western part of the Sichuan Basin and descending motion in the eastern part forms, leading to the highest cloud amount in China over the western part of the basin and a smaller cloud amount over the eastern part. It seems that the cloud center simulated by the AREM is reasonable and more delicate than that of the ISCCP data.

The top height of the stratiform clouds may be determined by the strength of the upward motion and the circulation condition in the middle troposphere. Impacted by the topography effect of the Tibetan Plateau, a mid-level divergence layer, which has been verified by ECWMF reanalysis data (Yu et al., 2001), is maintained over EC in winter. The model also presents that the westerlies over the plateau accelerate on their

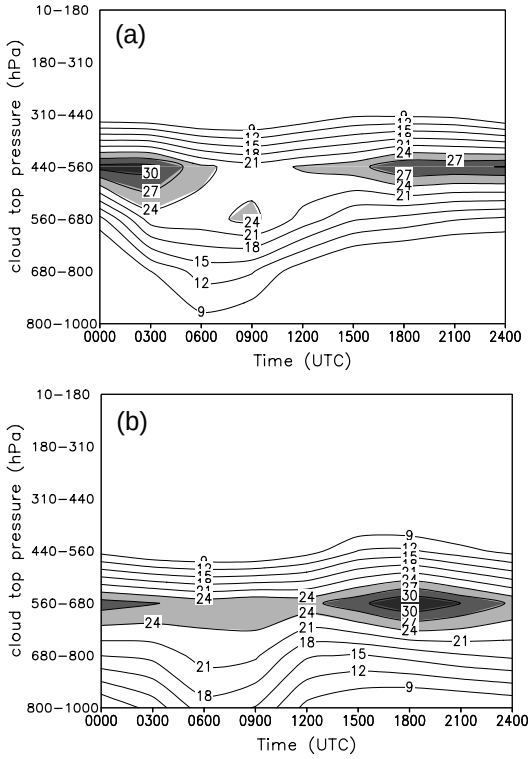

Fig. 5. Diurnal cycle of monthly mean vertical cloud fraction (in %) averaged over SG region in February 2001 derived from (a) the ISCCP D1 data and (b) the AREM model. Values larger than 24% are shaded.

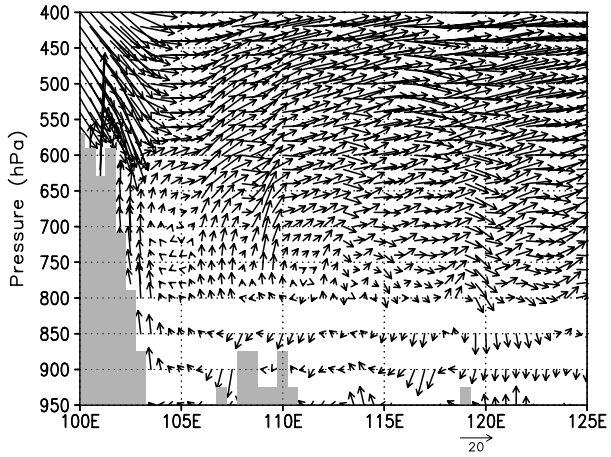

Fig. 6. Cross section of the monthly mean vector of the zonal wind in m s^{-1} and vertical velocity in 10^2 Pa s^{-1} along 30°N in February 2001 derived from the AREM model.

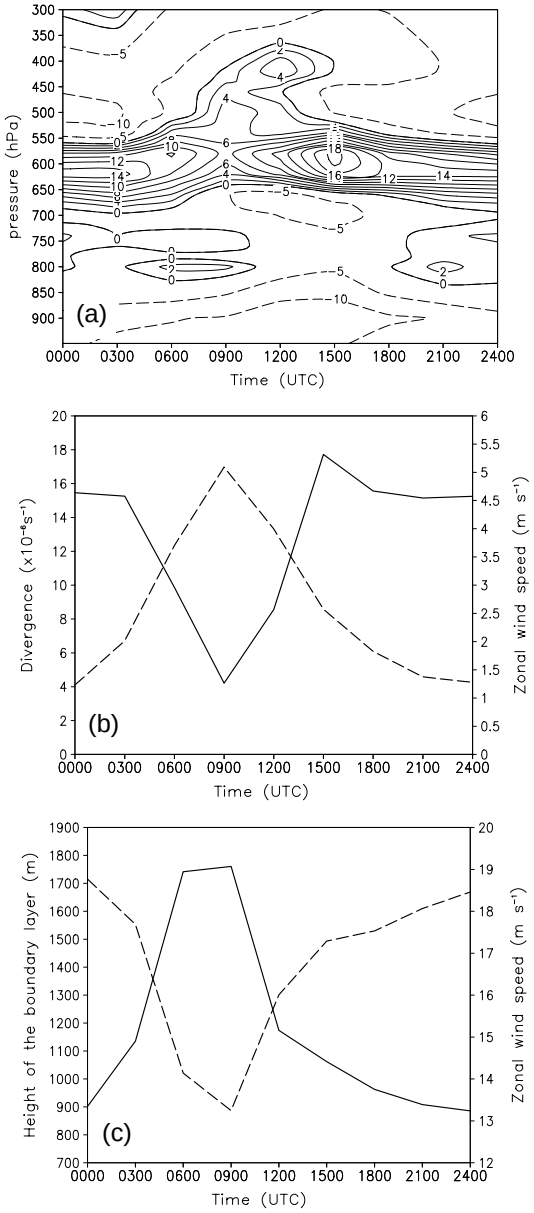

Fig. 7. (a) Diurnal cycle of monthly mean divergence (in s^{-1}) as a function of pressure averaged over SG region in February 2001 derived from the AREM model. Values greater than zero are indicated by solid lines, and those smaller than zero are dashed. (b) Diurnal changes of monthly mean divergence (in 10^6 s^{-1}, solid line, left coordinate) averaged over the SG region and zonal wind speed (in m s^{-1}, dashed line, right coordinate) averaged over the region (28°–32°N, 95°–102.5°E) at 620 hPa in February 2001 derived from the AREM model. (c) Diurnal changes of monthly mean height of the boundary layer (in m, solid line, left coordinate) and zonal wind speed (in m s^{-1}, dashed line, right coordinate) at 500 hPa averaged over the region (28°–32°N, 95°–102.5°E) in February 2001 derived from the AREM model.

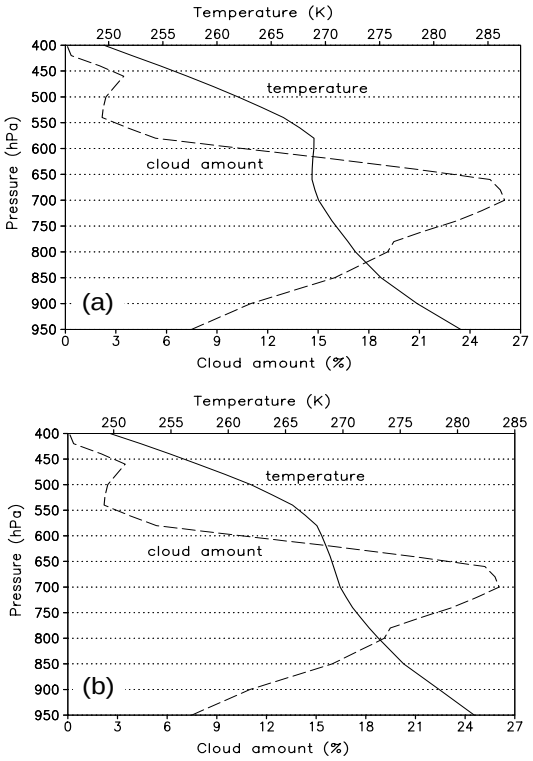

Fig. 8. Monthly mean temperature in K (solid line, top coordinate) and cloud fraction in % (dashed line, bottom coordinate) as a function of pressure averaged over SG region at (a) 0300 UTC and (b) 1500 UTC in February 2001 derived from the AREM model.

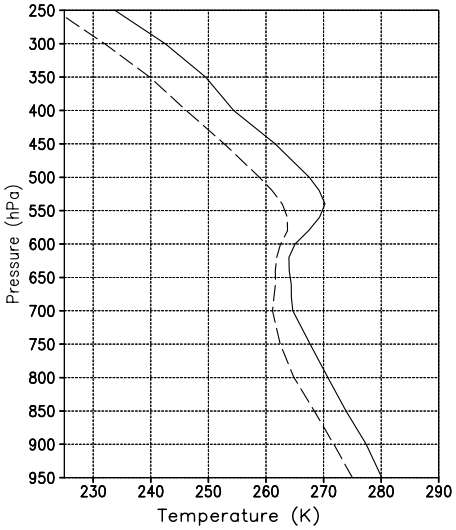

Fig. 9. Vertical profiles of three-day mean (averaged from 1 to 3 February 2001) temperature (solid line) and dew point (dashed line) in K as a function of pressure at Chengdu station (30.40°N, 104.01°E, 507.3 m) derived from the radiosonde data.

way away from the plateau, giving rise to large-scale, mid-level divergence over EC. The farther away from

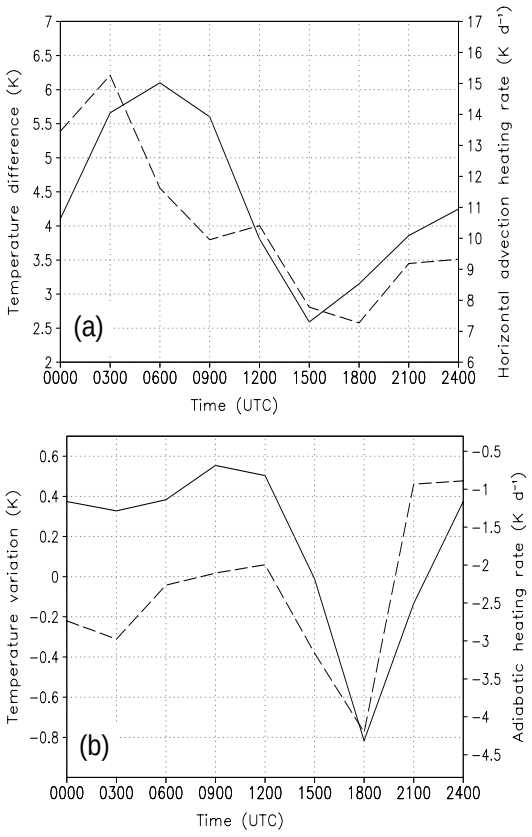

Fig. 10. (a) Diurnal changes of three-day mean (averaged from 1 to 3 February 2001) temperature difference between 560 hPa and 640 hPa (in K, solid line, left coordinate) and horizontal temperature advection heating rate (in K d^{-1}, dashed line, right coordinate) at 600 hPa averaged over SG region derived from the AREM model. (b) Diurnal changes of three-day mean (averaged from 1 to 3 February 2001) 3-hour interval temperature variation (in K, solid line, left coordinate) and adiabatic heating rate (in K d^{-1}, dashed line, right coordinate) at 640 hPa averaged over SG region derived from the AREM model.

the plateau, the weaker the horizontal wind shear and the smaller the divergence; the divergence becomes very small east of 110°E. To better illustrate the diurnal cycle of the divergence, Fig. 7a shows the monthly mean divergence in the core area, the SG region. A divergence center occurs at 640–620 hPa, with a maximum at 1500 UTC at night. In the daytime, the divergence minimizes and the height rises simultaneously. The intensity of the divergence, which is expressed by the difference between the westerly speed over the plateau and that in the free atmosphere over EC, may be determined by the boundary activities of the Tibetan Plateau. Figure 7b illustrates the diurnal

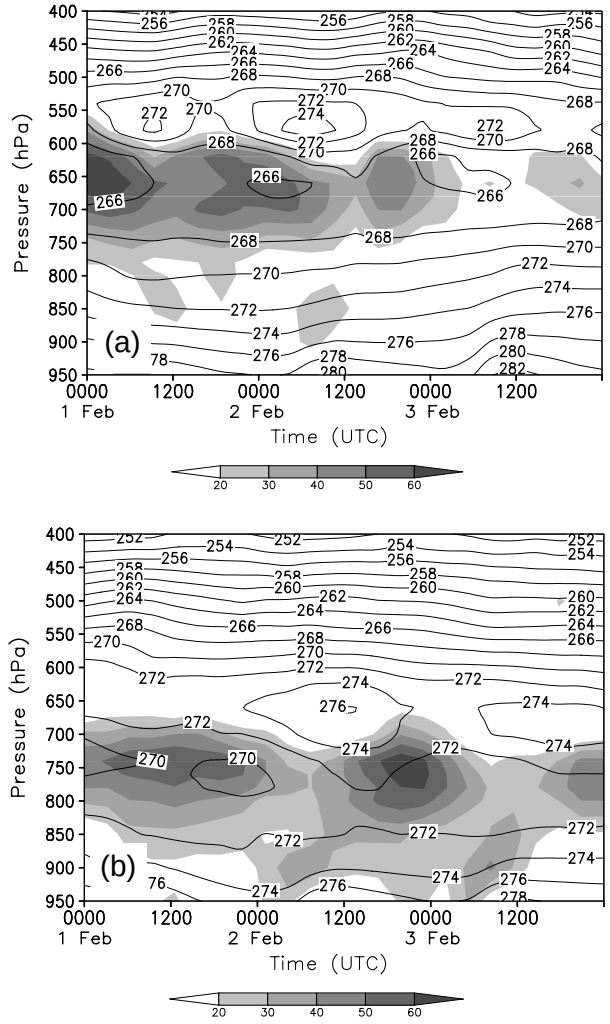

Fig. 11. Vertical distribution of temperature in K (solid contours) and cloud fraction in % (shaded) averaged over SG region from 1 to 3 February 2001 derived from (a) control experiment and (b) EXPT I.

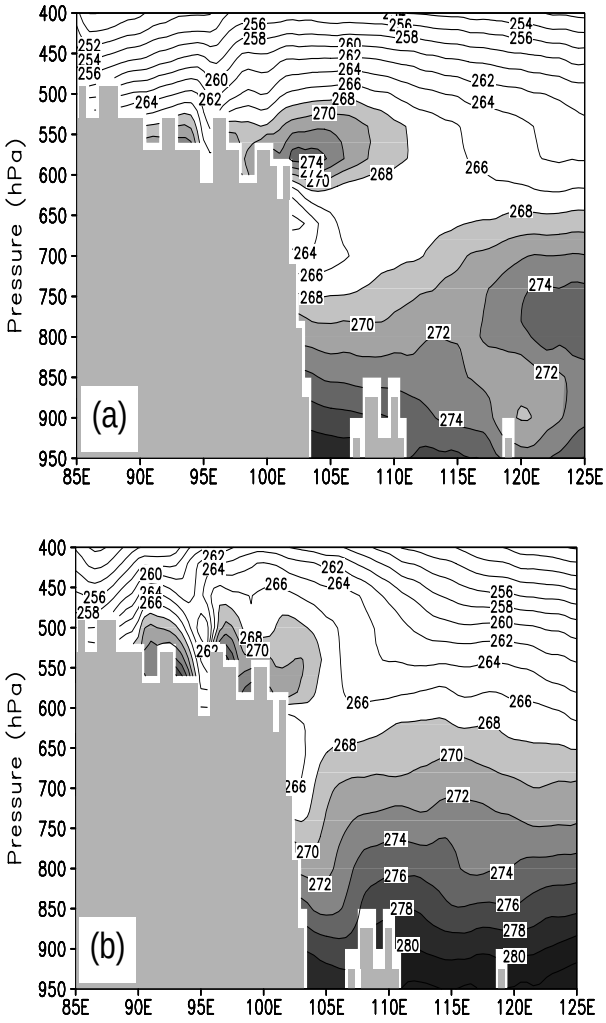

Fig. 12. Vertical-zonal cross section along 30°N of three-day mean (averaged from 1 to 3 February 2001) temperature in K derived from (a) control experiment and (b) EXPT II.

changes of the divergence in the core region and the zonal wind speed over the plateau at 620 hPa. Figure 7c shows the diurnal cycle of the monthly mean height of the boundary layer and the wind speed at 500 hPa over the eastern part of the plateau. Over the Tibetan Plateau, with the boundary activities strengthening in the daytime, the height of the boundary layer rises and momentum at the higher levels is transported to the lower levels, resulting in an increasing wind speed near the plateau surface (Fig. 7b) and a decreasing wind speed at the upper levels of the boundary layer (Fig. 7c). Because of the very weak diurnal change of the wind speed in the free atmosphere over SG the wind speed difference between these two regions decreases at the lower levels and increases at the upper levels (about 500 hPa) in the daytime, resulting in weak divergence and a higher divergence layer. At night, the boundary activities act in the opposite way, leading to strong divergence and a lower divergence height. The mid-level divergence layer may limit the cloud development, making EC become the largest continental middle cloud amount center in the world in the cold seasons.

The middle cloud amount may be influenced by the intensity of the divergence. When divergence is strong at night, the vertical velocity increases. Abundant water vapor can be brought to middle levels, giving rise to the increasing of the middle cloud amount. But during the day, the divergence is weak and the vertical velocity decreases, and middle cloudiness decreases simultaneously.

4.2 *Thermodynamic field in the middle troposphere*

Cloud development is limited not only by a divergence layer, but also by an inversion layer in the middle troposphere over EC. In general, in the daytime, the near surface temperature over the plateau (over the slope of the plateau) is higher than that of the free atmosphere at the same height due to sensible heating. The warm temperature advection from the Tibetan Plateau should be responsible for the mid-level inversion layer on the lee side of the Plateau. The inversion layer usually forms over the region 102.5°–110°E at 640–560 hPa, the same height as the plateau surface, being strong in the day and weak or faded at night. When the inversion is strong, clouds are suppressed below the inversion layer. Over the regions far away from the plateau, the inversion layer is thin or absent, and clouds can develop to higher levels. Because of the different intensity and thickness of the inversion layer at different times, inversion cannot be easily found from the monthly mean data. However, with the distinct diurnal change, it can be identified in the daytime. Figures 8a and 8b show the simulated monthly mean vertical structures of temperature and cloud amount over SG region at 0300 UTC (daytime) and 1500 UTC (nighttime) in February 2001, respectively. Figure 8a illustrates an inversion layer at 640–560 hPa, and a peak of the cloud amount appears beneath the inversion layer. Above the inversion, temperature drops rapidly with increasing height. But in Fig. 8b, no inversion layer occurs, temperature decreases gently from lower to higher levels, and the maximum cloud amount occurs a bit higher than in Fig. 8a. The mid-level inversion over the lee side of the plateau can be verified by the radiosonde data. Figure 9 shows an apparent inversion layer at 620–540 hPa in the three-day mean (from 1 to 3 February 2001, during which the model demonstrates an apparent mid-level inversion layer) vertical profiles of temperature and dew point at Chengdu station (30.40°N, 104.01°E, 507.3 m). The agreement between the simulation and observation confirms the existence of the mid-level inversion layer, and enhances the reliability of the model results.

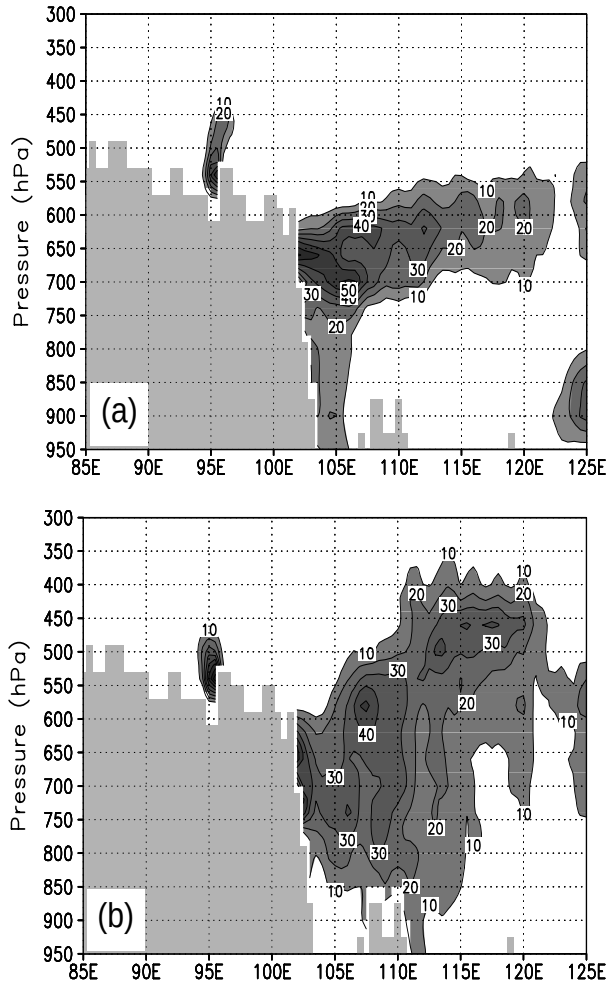

Fig. 13. Vertical-zonal cross section along 30°N of three-day mean (averaged from 1 to 3 February 2001) cloud fraction in % derived from (a) control experiment and (b) EXPT II. Values larger than 10% are shaded.

Beneath the inversion capping layer, a small cold center (see Fig. 12a) is located close to the eastern slope of the plateau. Adiabatic cooling of the ascending air may be responsible for the cold center. In Figs. 10a and 10b, the model results on 1 to 3 February 2001 are shown to explain the formation of the warm capping and cold center. Figure 10a shows similar diurnal cycles of the inversion and the horizontal temperature advection heating rate at inversion center height (about 600 hPa) over the lee side of the plateau. Because the change of the temperature may lag behind the advection, the fact that the maximum advection occurs at 0300 UTC whereas the strongest inversion appears at 0600 UTC is reasonable. Figure 10b shows that the 3-h interval temperature variation coincides with that of the adiabatic cooling rate at the cold center height (about 640 hPa) over the lee side of the plateau, which confirms that the cold center mainly results from the adiabatic cooling of the upward moving air. The diurnal cycle of the cooling rate and the divergence are in phase. When the divergence increases (decreases) at night (during the day), the vertical velocity is strengthened (weakened), resulting in stronger (weaker) adiabatic cooling.

In addition, two sensitivity experiments are designed to study the topography effects of the Tibetan

Plateau on the inversion. The control experiment is integrated from 0000 UTC 31 January to 2400 UTC 3 February 2001, and outputs of the first day are not analyzed. The same integration, except that the model topography is reduced to 2/3 of the height in the control run, is called sensitivity experiment 1 (hereinafter EXPT I). Figures 11a and 11b show the vertical structures of the temperature and cloud amount over the leeside of the Plateau simulated by the control run and EXPT I, respectively. In the control experiment, a persistent inversion layer is maintained at 640–560 hPa during these three days. When the inversion is weak, clouds can develop into lower levels of the inversion layer, but when it is strong, clouds may be limited beneath the bottom of the inversion layer. Figure 11b reproduces the same features as Fig. 11a except for the lower inversion layer and the cloud layer. EXPT I indicates that the height of the inversion layer over EC may be determined by the elevation of the Tibetan Plateau. To further verify the effect of the warm air transport on the inversion, advection terms (both horizontal and vertical) in the thermodynamic equation in the control run are neglected in a simulation called EXPT II. Figures. 12a and 12b show the mean vertical distributions of the temperature along 30°N of the control run and EXPT II, respectively. Figure 12b shows a much weaker inversion than that in Fig. 12a in the middle troposphere. Furthermore, when the horizontal temperature advection term is neglected alone in the equation, the mid-level inversion layer nearly disappears (not shown). With weak inversion in EXPT II, clouds can develop to higher levels (Fig. 13b) than in the control run (Fig. 13a), which also confirms that the inversion layer does limit the cloud development in the vertical. Other factors, such as horizontal diffusion, grid-scale condensation heating, and longwave radiation cooling at the top of clouds, may also produce some influences on the inversion, but these are much weaker compared with the horizontal advection warming. With the stronger mid-level inversion and smaller vertical velocity in the daytime, the water vapor cannot be easily transported to higher levels, resulting in a lower cloud top during the day than at night.

5. Conclusions

Combining the explicit prognostic cloud scheme, the diagnostic cloudiness scheme and the ISCCP cloud simulator, a detailed cloud diagnostic module is established in the AREM. The dynamic and thermodynamic conditions for middle cloud formation are studied and the performance of the AREM on cloud features over EC in February 2001 is examined quantitatively. Our main conclusions are as follows.

(1) The model simulations confirm that the divergence resulting from the blocking and friction of the plateau provides a favorable dynamical environment for the mid-level clouds over EC. It is found that the inversion resulting from the warm transportation over the plateau also provides a favorable thermodynamic environment for the middle clouds.

(2) The mid-level divergence and inversion over EC display individual diurnal cycles, which may be determined by the boundary activities of the Tibetan Plateau. In the daytime, the increase of the wind speed at lower levels and the decrease at upper levels of the boundary layer cause smaller divergence and a higher divergence layer, and the reverse at night. Meanwhile, the enhancement of the warm advection from the plateau during the day results in stronger inversion, and the reverse at night.

(3) The cloud top height is mainly determined by the strength of the inversion, and the middle cloud amount is mainly influenced by the intensity of the divergence.

Although cloud processes over EC are well reproduced by the AREM model, some discrepancies in cloud amount and cloud top height are found in the simulations. The cloud amount is much smaller than the ISCCP data over most Chinese regions, the cloud height is lower and cloud optical depth is thicker than observation. These discrepancies should be studied further, and efforts should be devoted to the improvement of the cloud parameterization.

Acknowledgments. The authors are grateful to two anonymous reviewers whose constructive comments have greatly improved the revised manuscript. The ISCCP dataset and ISCCP cloud simulator were downloaded from the website (http://isccp.giss.nasa.gov). This work was jointly supported by the National Key Basic Research and Development project of China under Grant No. 2004CB418304 and the National Natural Science Foundation of China under Grant Nos. 40233031 and 40221503.

REFERENCES

Betts, A. K., 1986: A new convective adjustment scheme, Part I: Observational and theoretical basis. *Quart. J. Roy. Meteor. Soc.*, **112**, 677–691.

Dai Yongjiu, and Zeng Qingcun, 1998: A land-surface model (IAP94) for climate studies, Part I: Formation and validation in off-line experiments. *Adv. Atmos. Sci.*, **14**, 433–460.

Doutriaux-Boucher, M., and G. Seze, 1998: Significant changes between the ISCCP C and D cloud. *Climatologies. Geophys. Res. Lett.*, **25**, 4193–4196.

Edwards, J. M., and A. Slingo, 1996: Studies with a flexible new radiation code. I: Choosing a configuration for a large-scale model. *Quart. J. Roy. Meteor. Soc.*, **122**, 689–719.

Holtslag, A. A. M., and B. A. Boville, 1993: Local versus nonlocal boundary-layer diffusion in a global climate model. *J. Climate*, **6**, 1825–1842.

Ju Lixia, Lei Xiaoen, and Han Zhiwei, 2003: Nested meteorological model system for air pollution prediction. *Journal of the Graduate School of the Chinese Academy of Sciences*, **20**, 470–476. (in Chinese)

Klein, S. A., and D. L. Hartmann, 1993: The seasonal cycle of low stratiform clouds. *J. Climate*, **6**, 1587–1606.

Li Yunying, Yu Rucong, Xu Youping, and Zhang Xuehong, 2003: The formation and diurnal changes of stratiform clouds in southern China. *Acta Meteorologica Sinica,* **61**, 733–743. (in Chinese)

Li, Y. Y., R. C. Yu, Y. P. Xu, and X. H. Zhang, 2004: Spatial distribution and seasonal variation of cloud over China based on ISCCP data and surface observations. *J. Meteor. Soc. Japan*, **82**, 761–773.

Lin, W. Y., and M. H. Zhang, 2004: Evaluation of clouds and their radiative effects simulated by the NCAR Community Atmospheric Model CAM2 against satellite observations. *J. Climate,* **17**, 3302–3318.

Morcrette, J.-J., and Y. Fouquart, 1986: The overlapping of cloud layers in short radiation parameterizations. *J. Atmos. Sci.*, **4**, 321–328.

Reynolds, R. W., N. A. Rayner, T. M. Smith, D. C. Stokes, and W. Wang, 2002: An improved in situ and satellite SST analysis for climate. *J. Climate*, **15**, 1609–1625.

Rossow, W. B., and R. A. Schiffer, 1991: ISCCP cloud data products. *Bull. Amer. Meteor. Soc.*, **72**, 2–20.

Rossow, W. B., and R. A. Schiffer, 1999: Advances in understanding clouds from ISCCP. *Bull. Amer. Meteor. Soc.*, **80,** 2261–2287.

Siebesma, A. P., and Coauthors, 2003: A large eddy simulation intercomparison study of shallow cumulus convection. *J. Atmos. Sci.*, **60**, 1201–1219.

Sun, Z. A., and L. Rikus, 1999: Improved application of exponential sum fitting transmissions to inhomogeneous atmosphere. *J. Geophys. Res.,* **104D**, 6291–6303.

Weare, B. C., 2004: A comparison of AMIP II model cloud layer properties with ISCCP D2 estimates. *Climate Dyn.*, **22**, 281–292.

Webb, M., C. Senior, S. Bony, and J.-J. Morcrette, 2001: Combining ERBE and ISCCP data to assess clouds in the Hadley Center, ECMWF and LMD atmospheric climate models. *Climate Dyn.*, **17**, 905–922.

Williams, K. D., M. A. Ringer, and C. A. Senior, 2003: Evaluating the cloud response to climate change and current climate variability. *Climate Dyn.*, **20**, 705–721.

Xu, K. M., and D. A. Randall, 1996: A semiempirical cloudiness parameterization for use in climate models. *J. Atmos. Sci.*, **53**, 3084–3102.

Xu Youping, Xia Daqing, and Qian Yueying, 1998: The water-bearing numerical model and its operational forecasting experiments. Part II: The operational forecasting experiments. *Adv. Atmos. Sci*, **15**, 321–336.

Yu Rucong, 1994: Two-step shape-preserving advection scheme. *Adv. Atmo. Sci*, **11**, 479–490.

Yu Rucong, Zeng Qingcun, Peng Guikang, and Chai Fuxing, 1994: Research on "Ya-An-Tian-Lou". Part II: Numerical trial forecasting. *Chinese J. Atmos. Sci.*, **13**, 145–158. (in Chinese)

Yu Rucong, Yu Yongqiang, and Zhang Minghua, 2001: Comparing cloud radiative properties between the eastern China and the Indian monsoon region. *Adv. Atmos. Sci*, **18**, 1090–1102.

Yu Rucong, Xue Jishan, and Xu Youping, 2004: *AREMS Meso-scale Heavy Rainfall Numerical Prediction Model System.* China Meteorological Press, Beijing, 232pp. (in Chinese)

Zhang Liping, Chen Wanchun, Xia Jun, Niu Cunwen, and Song Xingyuan, 2003: Numerical simulation study on developing process of drought disaster. *Engineering Journal of Wuhan University*, **36**, 24–27. (in Chinese)

Zhong Xiaoping, and Qing Qingtao, 2001: Numerical simulation of precipitation in the eastern Tibetan Plateau with LASG mesoscale model and its operational application evaluation. *Quarterly Journal of Applied Meteorology*, **12**, 167–175. (in Chinese)